PHYSICAL REVIEW A **88**, 023602 (2013)

Dynamics of spin-1 bosons in an optical lattice: Spin mixing, quantum-phase-revival spectroscopy, and effective three-body interactions

K. W. Mahmud and E. Tiesinga

Joint Quantum Institute, National Institute of Standards and Technology and University of Maryland, 100 Bureau Drive, Gaithersburg, Maryland 20899, USA

(Received 29 April 2013; published 5 August 2013)

We study the dynamics of spin-1 atoms in a periodic optical-lattice potential and an external magnetic field in a quantum quench scenario where we start from a superfluid ground state in a shallow lattice potential and suddenly raise the lattice depth. The time evolution of the nonequilibrium state shows collective collapse-and-revival oscillations of matter-wave coherence as well as oscillations in the spin populations. We show that the complex pattern of these two types of oscillations reveals details about the superfluid and magnetic properties of the initial many-body ground state. Furthermore, we show that the strengths of the spin-dependent and spin-independent atom-atom interactions can be deduced from the observations. The Hamiltonian that describes the physics of the final deep lattice not only contains two-body interactions but also effective multibody interactions, which arise due to virtual excitations to higher bands. We derive these effective spin-dependent three-body interaction parameters for spin-1 atoms and describe how spin mixing is affected. Spinor atoms are unique in the sense that multibody interactions are directly evident in the *in situ* number densities in addition to the momentum distributions. We treat both antiferromagnetic (e.g., ^{23}Na) and ferromagnetic (e.g., ^{87}Rb and ^{41}K) condensates.

DOI: 10.1103/PhysRevA.88.023602 PACS number(s): 03.75.Mn, 03.75.Kk, 67.85.Fg

I. INTRODUCTION

Quantum degenerate ultracold atoms with a spin degree of freedom exhibit both magnetic order and superfluidity, offering a rich system in which to explore quantum coherence, long-range order, magnetism, and symmetry breaking. Many aspects of spinor atoms in a trap have been investigated with spin $F = 1$ atoms, such as ^{23}Na and ^{87}Rb [1–5]. Spin $F = 2$ [6–8] and $F = 3$ [9,10] spinor gases have been studied to a lesser extent. Spinor condensates are described by a vector order parameter [11–13]. The distinctive feature is its spin-dependent interaction which organizes spins, giving rise to ferromagnetic and antiferromagnetic (polar) order. It can also coherently convert a spin $m = 1$ and a $m = -1$ atom to a pair of $m = 0$ atoms, and vice versa [14–16], while conserving magnetization and energy.

In parallel with the exploration of ultracold spinor physics, optical lattices have become a powerful tool to create strongly correlated many-body states of bosons and fermions [17–21]. Lattice systems offer flexibility as the lattice parameters and particle interactions can be controlled easily, thereby facilitating progress towards the creation of quantum emulators [22,23]. Since the observation of the superfluid to Mott insulator transition with spinless bosons [18], steady progress has been made towards the understanding of spinor atoms in an optical lattice [24–26]. Issues of temperature and entropy [27] are among the challenges that need to be overcome to create a many-body correlated state of spin-1 atoms. Theoretical studies of lattice-trapped spinor condensates have mainly explored the phase diagram and the nature of the superfluid–Mott insulator transition [28–33].

Due to the tunability of cold atom and optical lattice parameters, it is also possible to study nonequilibrium dynamics. Dynamics of many-body quantum systems is still an emerging field, and only a few issues have been investigated [34]. An early experiment [35] studied the dynamics of spinless bosons in a suddenly raised optical lattice, observing the collapse and revival of the matter-wave field in the momentum distribution. In a more recent experiment [36], tens of oscillations in the momentum distribution or visibility were observed, and the predicted [37] signature of effective many-body interactions confirmed. As for spin-1 atoms, dynamical studies have mainly focused on large atom number continuum or trapped systems in the mean field regime, exploring spin-mixing dynamics [14,15], quantum quench dynamics [38,39], and various instabilities [40].

The goal of this paper is to study the dynamics of spin-1 bosonic atoms in a three-dimensional (3D) optical lattice and probe its many-body state and system properties. Starting with a ferromagnetic (^{87}Rb) or antiferromagnetic (^{23}Na) superfluid ground state in a shallow lattice, suddenly raising the lattice depth creates a nonequilibrium state which can be followed in various scenarios—with and without a magnetic field, and with and without effective three-body interactions. The evolution shows collapse and revival of matter-wave coherence measured by visibility oscillations, in a more complex pattern than for spinless bosons [35,41]. It also shows oscillations in spin populations due to the combined effect of the spin-mixing collisions of the $m = 0$ and $m = \pm 1$ components and differential level shifts proportional to the square of the magnetic field strength, the quadratic Zeeman shift. Linear Zeeman shifts do not affect the behavior of spinor condensates. Both spin mixing and visibility oscillations reveal details about the system such as the composition of the initial many-body state, and thereby its superfluid and magnetic properties.

By analyzing the frequency spectrum of the visibility, we show that the ratio U_2/U_0 of spin-dependent and spin-independent atom-atom interactions can be deduced. Combined with spectra of spin-mixing dynamics at various magnetic field strengths, this gives us a method to measure the interaction couplings for spin-1 atoms. Finally, we find that the

presence of a quadratic Zeeman shift enhances spin-mixing oscillations for ferromagnets and shows collapse and partial revivals in the transverse magnetization.

The Hamiltonian that quantitatively describes the physics of the final deep lattice is comprised of two-body as well as effective multibody interactions, which arise due to virtual excitations to higher bands. We derive the induced three-body interaction parameters for spin-1 atoms in a deep harmonic well, approximating the minimum of a single lattice site as such, and find the existence of *spin-dependent* three-body interactions. We show how to detect the signature of the three-body interactions and argue that they are directly exhibited in the *in situ* density as opposed to the time-of-flight visibility measurements, as is the case for spinless bosons [36].

The article is organized as follows. In Sec. II we set up the spin-1 Bose-Hubbard model, sketch the mean-field theory to determine the initial ground state, describe the exact Hamiltonian after the quench, and discuss observables and computational aspects. We present our main results in Secs. III, IV, and V. Section III explores the nonequilibrium dynamics of antiferromagnetic spin-1 atoms, with and without a magnetic field. Section IV describes the dynamics for a ferromagnetic spinor. Section V shows the effects of effective three-body interactions in the dynamics. We summarize our results and discuss the limitations of our simulations in Sec. VI. A derivation of the effective three-body interaction is given in the Appendix.

II. MODEL AND COMPUTATIONAL ASPECTS

A. Shallow lattice Hamiltonian

Ultracold spin-1 bosons in the lowest band of a 3D cubic optical lattice and an external magnetic field B along the z axis are modeled by the free energy

$$\begin{aligned} H = & -J \sum_{\langle i,j\rangle,m} (a_{im}^\dagger a_{jm} + a_{jm}^\dagger a_{im}) + \frac{U_0}{2} \sum_i \hat{n}_i (\hat{n}_i - 1) \\ & + \frac{U_2}{2} \sum_i (\vec{\hat{\mathcal{F}}}_i \cdot \vec{\hat{\mathcal{F}}}_i - 2\hat{n}_i) + \delta \sum_{im} m^2 a_{im}^\dagger a_{im} \\ & - \mu \hat{N} - \mu_M \hat{M} \,. \end{aligned} \tag{1}$$

Here $a_{im}^\dagger$ is the creation operator of a boson in magnetic sublevel $m = -1$, 0, or 1 in the energetically lowest Wannier function or orbital of lattice site i. The first term in Eq. (1) represents the hopping of atoms between nearest-neighbor sites $\langle i,j\rangle$ and is proportional to the hopping energy J. The second term describes the on-site atom-atom repulsion with strength $U_0 > 0$, $\hat{n}_i = \sum_m \hat{n}_{im}$, and $\hat{n}_{im} = a_{im}^\dagger a_{im}$. The third term is a spin-dependent atom-atom interaction with a strength U_2 that can be either positive (antiferromagnetic) or negative (ferromagnetic). The three operators $\vec{\hat{\mathcal{F}}}_i = (\hat{\mathcal{F}}_{xi}, \hat{\mathcal{F}}_{yi}, \hat{\mathcal{F}}_{zi})$ on site i satisfy angular momentum commutation rules and are defined by $\hat{\mathcal{F}}_{qi} = \sum_{m,m'} a_{im}^\dagger (F_q)_{mm'} a_{im'}$ for $q = x$, y, or z, and $(F_q)_{mm'}$ are matrix elements m, m' of component α of the spin-1 angular momentum $\vec{F}$. The fourth term corresponds to the quadratic Zeeman energy of the magnetic sublevels with strength δ. Finally, the terms containing the Lagrange multipliers μ and μ_M control the total atom number, $\hat{N} = \sum_i \hat{n}_i$, and total magnetization, $\hat{M} = \sum_i \hat{m}_i$, respectively. Here $\hat{m}_i \equiv \hat{\mathcal{F}}_{zi} = \sum_m m \hat{n}_{im}$ is the on-site magnetization. Both $\hat{N}$ and $\hat{M}$ commute with H. (The large linear Zeeman Hamiltonian of the atoms is "absorbed" in the term $-\mu_M \hat{M}$ and is seen not to affect the physics of the spinor condensate.)

The interaction strengths are given by $U_0 = 4\pi\hbar^2\bar{n}(a_0 + 2a_2)/(3M_a)$ and $U_2 = 4\pi\hbar^2\bar{n}(a_2 - a_0)/(3M_a)$ [11], where a_F with $F = 0$ or 2 are scattering lengths for the two allowed values of the total angular momentum of s-wave collisions of two spin-1 particles at zero collision energy and zero magnetic field. S-wave scattering with total angular momentum $F = 1$ is prohibited due to bosonic wave function symmetry. The mean density of the local orbital $\bar{n}$ is determined by the laser parameters and polarizability of the atom. Finally, M_a is the mass of the atom, $\hbar = h/(2\pi)$, and h is Planck's constant.

The ratio of the two interaction strengths is independent of lattice parameters as the $\bar{n}$ dependence cancels. For ^{23}Na, $U_2/U_0 = +0.036(3)$ [42] and the system is antiferromagnetic. For ^{87}Rb, $U_2/U_0 = -0.004\,6(7)$ [43] and the system is ferromagnetic. The quoted uncertainty in U_2/U_0 for ^{23}Na and ^{87}Rb is one standard deviation, obtained from the corresponding references. For ^{41}K we find $U_2/U_0 = -0.026$ [44,45]. For our investigation we use $U_2/U_0 = 0.04$ for sodium and -0.005 for rubidium. The quadratic Zeeman strength $\delta = \delta_0 B^2$ with $\delta_0/h = 27.68$ Hz/(mT)^2 for ^{23}Na and $\delta_0/h = 7.189$ Hz/(mT)^2 for ^{87}Rb.

The phase diagram for the spin-1 Bose-Hubbard model in one-dimension has been calculated with numerical methods such as quantum Monte Carlo [31] and density matrix renormalization group [46]. Mean-field approaches for spin-1 bosons, which give predictions for any dimension, have also been performed [32,47,48] and are extensions of those for scalar bosons [49,50]. As mean-field models are most predictive in three dimensions and we focus on such a lattice, we use the decoupling mean-field theory [32] to find the initial many-body ground state.

In a mean-field approximation, the hopping term in Eq. (1) can be decoupled as

$$a_{im}^\dagger a_{jm} \simeq \langle a_{im}^\dagger \rangle a_{jm} + a_{im}^\dagger \langle a_{jm} \rangle - \langle a_{im}^\dagger \rangle \langle a_{jm} \rangle \,, \tag{2}$$

when fluctuations around the equilibrium value are negligible. We can define $\psi_m = \langle a_{jm} \rangle$, for $m = 1, 0, -1$, as the site-independent superfluid order parameter. Using Eq. (2) we can rewrite Eq. (1) as a sum of independent single-site Hamiltonians, $H = \sum_i H_i^{\rm mf}$, where

$$\begin{aligned} H_i^{\rm mf} = & \frac{U_0}{2} \hat{n}_i (\hat{n}_i - 1) + \frac{U_2}{2} (\vec{\hat{\mathcal{F}}}_i \cdot \vec{\hat{\mathcal{F}}}_i - 2\hat{n}_i) \\ & + \delta \sum_m m^2 a_{im}^\dagger a_{im} - \mu \hat{n}_i - \mu_M \hat{m}_i \\ & - zJ \sum_m (\psi_m a_{im}^\dagger + \psi_m^* a_{im}) + zJ \sum_m |\psi_m|^2 \,, \end{aligned} \tag{3}$$

and z is the number of nearest neighbors, e.g., $z = 6$ in 3D. For a given μ and μ_M the superfluid order parameters and ground-state wave function are obtained by finding those values of ψ_m for which the energetically lowest eigenstate of $H_i^{\rm mf}$ is smallest.

The character of the ground state depends on whether the spin-dependent term U_2 is positive or negative [11]. For the antiferromagnetic $U_2 > 0$ superfluid ground states, the order parameters can be written as $\psi_m = \sqrt{\rho_s} e^{i\theta} D^1_{m0}(\alpha,\beta,\gamma)$, while for the ferromagnetic $U_2 < 0$ superfluid we have $\psi_m = \sqrt{\rho_s} e^{i\theta} D^1_{m1}(\alpha,\beta,\gamma)$. Here the functions $D^J_{MM'}(\alpha,\beta,\gamma)$ are Wigner rotation matrices [51], with Euler angles α, β, and γ determined by minimizing $H_i^{\rm mf}$. The real valued ρ_s and angle θ are the spin-independent superfluid density and a global phase, respectively. We have $\rho_s \leqslant \langle \hat{n} \rangle$.

Within mean-field theory the many-body superfluid wave function is given by the product wave function $\prod_i |\mathrm{GS}\rangle_i$ over sites i, where $|\mathrm{GS}\rangle = \sum_{\vec{n}} c_{\vec{n}} |\vec{n}\rangle$ and kets $|\vec{n}\rangle = |n_{-1}, n_0, n_1\rangle$ are elements of the *occupation-number* basis of Fock states of the three m projections. The single-site wave function is a superposition of Fock states with amplitudes $c_{\vec{n}}$. In fact, it is also a superposition of Fock states with different magnetization.

We present only results for homogeneous ground states with zero magnetization $\langle m_i \rangle = 0$ at every site, ensured by setting $\mu_M = 0$. Results for other magnetizations show similar physics. For $U_2 > 0$ the bosons condense into a state with $\langle \vec{\mathcal{F}}_i \rangle = 0$. This is called a polar (antiferromagnetic) superfluid. There are two kinds of polar order [32]: the ground state is a transverse polar state with $(\psi_{-1}, \psi_0, \psi_1) = \sqrt{\rho_s}(1,0,1)/\sqrt{2}$ when $\delta < 0$, and a longitudinal polar state with $(\psi_{-1}, \psi_0, \psi_1) = \sqrt{\rho_s}(0,1,0)$ when $\delta > 0$. For ferromagnetic atoms with $U_2 < 0$ the magnetic order maximizes the total angular momentum with $\langle \vec{\mathcal{F}}_i \rangle^2 = 1$ [11], leading to a partially magnetized superfluid with order parameters $(\psi_{-1}, \psi_0, \psi_1) = \sqrt{\rho_s}(1, \sqrt{2}, 1)/2$ for $0 < \delta < 2U_2$, and a longitudinal superfluid with order parameters $\sqrt{\rho_s}(0,1,0)$ for $\delta > 2U_2$.

Our numerical simulations are performed in the occupation number basis. Only basis functions with $n_{-1} + n_0 + n_1 \leqslant n_{max}$ are included. We use $n_{max} = 6$, leading to 84 basis functions in a site and negligible truncation errors when the mean atom number per site is less than three. All current optical-lattice experiments use mean atom numbers of this order of magnitude.

B. Deep lattice Hamiltonian

After preparing the initial superfluid, the depth of the optical lattice is suddenly increased so that tunneling is turned off. This lattice ramp up is assumed to be slow enough to prevent excitations to a higher band yet fast enough compared to interactions. We can then treat subsequent time evolution due to the single-site Hamiltonian

$$H^{\rm final} = \frac{U_0}{2}\hat{n}(\hat{n}-1) + \frac{U_2}{2}(\vec{\mathcal{F}}\cdot\vec{\mathcal{F}} - 2\hat{n}) + \delta \sum_m m^2 a_m^\dagger a_m \tag{4}$$

exactly. As each site evolves under the same Hamiltonian, we have suppressed the site index. For induced three-body interactions, additional terms appear in $H^{\rm final}$ as discussed in Sec. V. For a recent observation of multibody effects for lattice-trapped spinless bosons [36], where a similar quench was used, a mean-field treatment [37,52] of the initial state followed by exact on-site evolution was found to agree well with the experiment. If lattice sites are not completely decoupled ($J \neq 0$) during the evolution, a correlated multisite treatment is necessary [53]. We do not study that scenario in this paper.

Following Ref. [14] we realize that, in addition to the occupation number basis, eigenfunctions of the operators $\hat{n}$, $\vec{\mathcal{F}}^2 = \vec{\mathcal{F}}\cdot\vec{\mathcal{F}}$, and $\mathcal{F}_z$ also form a complete basis for the on-site Hilbert space of $H^{\rm final}$. In fact, these *angular-momentum* basis states $|n, F, M\rangle$ diagonalize $H^{\rm final}$ when $\delta = 0$ with energy spectrum

$$E^{\rm final}(\delta = 0) = \frac{U_0}{2} n(n-1) + \frac{U_2}{2}\left[F(F+1) - 2n\right], \tag{5}$$

where n is the local atom number and the quantum number F is restricted to $F \leqslant n$ and even(odd) F for even(odd) n. The integer M is the magnetization quantum number with $|M| \leqslant F$. For $\delta \neq 0$ the quadratic Zeeman interaction couples the angular-momentum basis states. Finding its matrix elements is involved, leading us to perform all simulations in the occupation number basis.

C. Observables

To analyze the nonequilibrium dynamics of our system, we follow several observables. The first is the atom number per lattice site in each spin component $\langle \hat{n}_{im} \rangle$, which can be detected either *in situ* [54] or, after release of the atoms from the lattice, by the Stern-Gerlach separation method where the spin states are first spatially separated and then detected [16]. The second observable is the visibility, which is a measure of coherence of the wave function and equals the number of atoms with zero momentum in the spin-dependent momentum distribution. This is the standard quantity measured after releasing atoms from the lattice and a time-of-flight expansion [36,55]. Within our simulation it is given by $|\langle \hat{a}_{im} \rangle|^2$ for any site i. Finally, we study the square of the *in situ* transverse magnetization $|\langle \hat{\mathcal{F}}_{ix} \rangle|^2$. Transverse magnetization can be measured by Faraday rotation spectroscopy, which allows for continuous observation of spin population in a BEC [2,56].

III. DYNAMICS OF AN ANTIFERROMAGNETIC SPINOR

A. Evolution without magnetic field

In this section we analyze the dynamics of a longitudinal polar superfluid ground state after the optical lattice strength is rapidly raised. The condensate evolves under $H^{\rm final}$, with $\delta = 0$ for hold time t, after which one or more of the observables is measured. Figure 1(a) shows the typical evolution of the *in situ* population of spin components $m = \pm 1, 0$ as a function of hold time. Here we use typical numbers for ^{23}Na atoms: in the initial lattice with $U_0/(zJ) = 2$, $U_2 = +0.04U_0$, and a mean atom-number per site of $\langle \hat{n} \rangle = 1.31$, and in the final lattice $U_0 = 0.1\hbar\omega_f, U_2 = +0.04U_0$, where ω_f is the harmonic frequency near the minima of the lattice potential. (An infinitesimal $\delta > 0$ is applied to ensure formation of the longitudinal polar state.)

Initially, all atoms are in the $m = 0$ state and as time evolves, atoms begin to appear in states $m = \pm 1$ because of spin-changing collisions, and a pattern of periodic modulation emerges with a period of h/U_2, while conserving zero magnetization. This spin-mixing time trace also contains information about the composition of the initial many-body

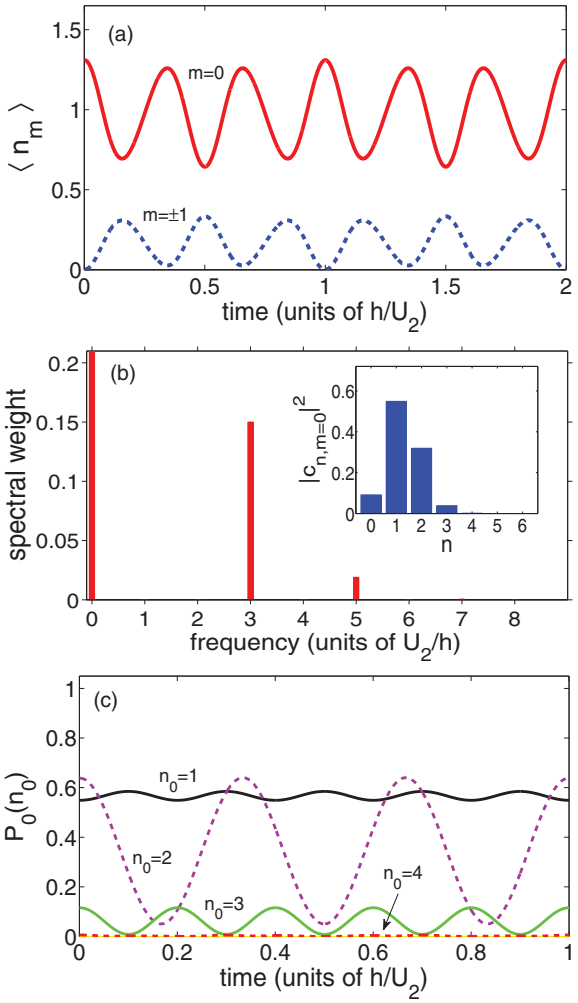

FIG. 1. (Color online) Spin-mixing dynamics after a sudden increase of lattice depth starting with the longitudinal antiferromagnetic ground state of spin-1 ^{23}Na in a zero magnetic field. (a) The on-site atom number of the spin components, $\langle \hat{n}_{m=0,\pm1} \rangle$, as a function of hold time showing spin mixing. Time is in units of h/U_2, and system parameters are described in the text. (b) Fourier spectrum of the time trace in (a) showing the frequencies involved in the spin-mixing dynamics. The inset shows the initial ground-state Fock-state number probabilities $|c_{\vec{n}=(0,n_0,0)}|^2$ as a function of atom number n_0 in spin component $m = 0$. Atom numbers with $m = \pm 1$ are vanishingly small. (c) Contribution P_0 to $\langle \hat{n}_{m=0} \rangle$ of having n_0 atoms in the $m = 0$ state, where $P_0(n_0) = \sum_{n_{m=\pm1}} n_0 |c_{\vec{n}}|^2$. The curves are for $n_0 = 1$, 2, 3, and 4, showing that the $3h/U_2$ periodicity is due to $n_0 = 2$ and $5h/U_2$ periodicity due to $n_0 = 1$ and 3, respectively.

state. To explore this, we further analyze the dynamics in Figs. 1(b) and 1(c). Figure 1(b) shows the Fourier analysis of the time trace in panel (a), and the inset shows on-site Fock state probabilities $|c_{\vec{n}}|^2$ for the initial state. The shape of the initial state number distribution is characteristic of a nearly coherent or a slightly squeezed state. In the frequency spectrum, peaks are observed at frequencies that are integer multiples of U_2/h. In fact, they occur at $3U_2/h$, $5U_2/h$, and a small contribution at $7U_2/h$. These features can be understood from an analysis of the eigenenergies in Eq. (5) of H^{final} at $\delta = 0$. Similar to number Fock state composition of the initial state, it is also a superposition of angular momentum states $|n, F, M\rangle$. The observables $\hat{n}_m$ commute with total atom number $\hat{n}$ and thus only measure the coherence between states with different F but the same n. For states with $n = 2$ the two allowed F are 0 and 2 with energy difference $3U_2$. This leads to a peak at $3U_2/h$ in Fig. 1(b). For $n = 3$ states, $F = 1$ and $F = 3$ exist, leading to the frequency at $5U_2/h$. The small feature at $7U_2/h$ indicates the presence and mixing of $|n, F, M\rangle = |4,4,0\rangle$ and $|4,2,0\rangle$ states. The above analysis of the eigenenergies is confirmed in Fig. 1(c). It depicts the time evolution of the contribution P_0 to $\langle \hat{n}_{m=0} \rangle$ of having n_0 atoms in the $m = 0$ state, where $P_0(n_0) = \sum_{n_{m=\pm1}} n_0 |c_{\vec{n}}|^2$. Atom number $n_0 = 2$ has a period of $(h/U_2)/3$ as we oscillate between states $|n_{-1}, n_0, n_1\rangle = |0,2,0\rangle$ and $|1,0,1\rangle$ with a total of two atoms, while that for $n_0 = 1$ and 3 has a period of $(h/U_2)/5$. Here, we oscillate between the three atom states $|n_{-1}, n_0, n_1\rangle = |0,3,0\rangle$ and $|1,1,1\rangle$.

The spin-mixing dynamics can be compared and contrasted with other spin-1 experiments. In Ref. [24], a pair of $F = 1$ ^{87}Rb atoms was prepared in a single site of a deep optical lattice in the Fock state $|0,2,0\rangle$ and allowed to spin mix with $|1,0,1\rangle$. Spin-mixing oscillations between two levels analogous to Rabi oscillations were observed with a single frequency. On the other extreme, spin mixing for a spinor Bose-Einstein condensate (BEC) with a large number of atoms has been discussed in theory and observed in experiments [14,15]. They are in a regime where a classical pendulum phase-space analysis is appropriate [57,58], and although there can be spin-mixing oscillations for specific initial states, quantum recurrences due to the discrete energy spectrum are absent. Our analysis here explores the regime which is between these two—the single Fock state regime and the regime of large atom number condensate. As such, we are exploring a regime which can shed light on the semiclassical transition to large condensate dynamics, a topic for future investigation. In our analysis here, we can analyze the multiple frequencies of the dynamics time trace to probe the composition and atom number statistics of the initial many-body state.

Figure 2 shows the dynamics of the visibility of the $m = 0$ state—the occupation of the zero-momentum state for the $m = 0$ component—for the same initial state and parameters as in Fig. 1. The visibility $|\langle a_{m=0}(t) \rangle|^2$ measures the phase coherence in this spinor superfluid system. We show the relative visibility $|\langle a_{m=0}(t) \rangle|^2 / |\langle a_{m=0}(t = 0) \rangle|^2$ in Fig. 2(a). We see that the atoms oscillate between being completely coherent to completely incoherent ($|\langle a_{m=0} \rangle|^2 \approx 0$). The pattern is more complex than the spinless boson visibility [35]. There is a fast oscillation with time scale $\sim h/U_0$, which is modified by a slower envelope with a time scale $\sim h/U_2$. The exact nature of the complex oscillations is revealed in the frequency spectrum shown in Fig. 2(b). Similar to Fig. 1, features appear at small integer multiples of U_2/h. Here they are located at $2U_2/h$, $3U_2/h$, and $5U_2/h$. Peaks also occur at much larger frequencies, with a dominant frequency at $(U_0 + U_2)/h$, which is $26U_2/h$ in this example. Twenty-six is also the number of fast oscillations in a full period h/U_2, as can be seen in panel (a). This indicates that for an unknown ratio U_2/U_0, one full revival of the oscillations of the visibility can help determine this ratio by counting the number of fast oscillations or equivalently, performing a frequency analysis. Combined

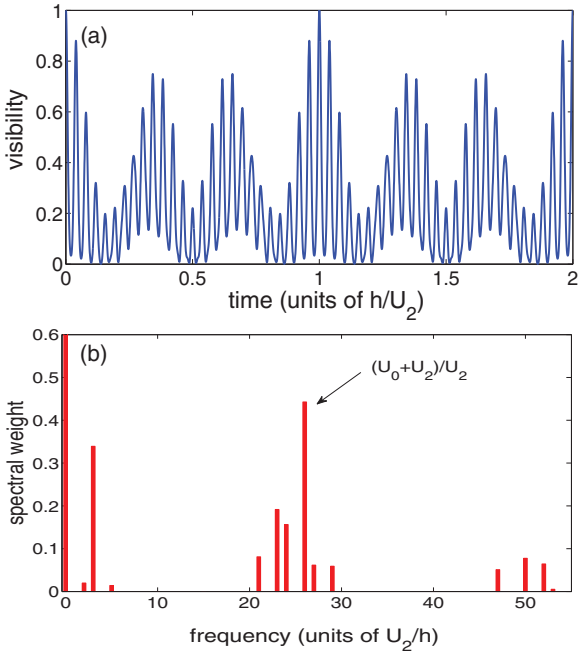

FIG. 2. (Color online) (a) Visibility $|\langle a_{m=0}(t)\rangle|^2/|\langle a_{m=0}(t=0)\rangle|^2$ of the $m=0$ state as a function of hold time t after a sudden increase of the lattice depth, for the same parameters as in Fig. 1. The pattern of collapse and revival of coherence is more complex than the spinless boson case due to the competition between spin-dependent and spin-independent interactions. There are U_0/U_2+1 fast oscillations in one full collapse and revival period of h/U_2, yielding a method to determine the ratio U_2/U_0 from visibility oscillations. (b) Spectrum of the visibility oscillations showing the range of contributing frequencies, the most dominant one being at $U_0/U_2+1=26$.

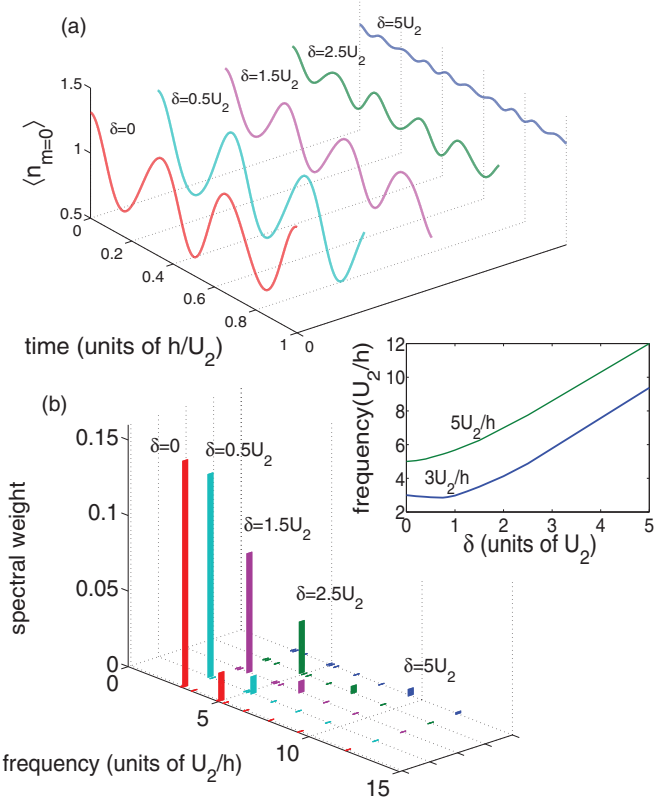

FIG. 3. (Color online) Spin-mixing oscillations in the presence of a magnetic field in the form of a quadratic Zeeman shift. Panel (a) shows the population in $m=0$ as a function of hold time for several values of the quadratic Zeeman shift. Panel (b) shows the frequency analysis of panel (a) with two dominant frequencies in the time evolution. At $\delta=0$ these frequencies are $3U_2/h$ and $5U_2/h$. The inset shows that the two dominant frequencies as a function of δ first dip before slowly increasing due to the competing nature of δ and U_2.

with the realization that this ratio is independent of lattice parameters, this method of determining spinor interactions is one of the key findings of this paper.

The visibility spectrum frequencies appear because the expectation value of the annihilation operator is sensitive to the overlap between Fock states of different atom numbers [36]. For example, $|n_{-1},n_0,n_1\rangle=|0,2,0\rangle$ connects to $|0,1,0\rangle$, giving rise to the dominant frequency U_0+U_2. Other frequencies can similarly be explained by performing an expansion of the initial state in the angular momentum basis, and applying the evolution operator for the final Hamiltonian Eq. (4) at $\delta=0$. For higher occupation numbers not shown here, we find that the visibility patterns become more complex. In fact, by controlling the initial squeezing [36,52] (i.e., by controlling the initial tunneling energy J) as well as the total occupation, we can change the complexity of the frequency spectrum and thereby make it amenable for analysis.

B. Effects of magnetic field

The energies of spin-1 atoms are sensitive to external magnetic fields. Such external fields have been exploited in manipulating spinor atoms in an optical trap—to access ground-state properties [1,2], in detection such as in the Stern-Gerlach separation method [16], or to influence the dynamics in quench experiments [39]. For spinor atoms in an optical lattice, external magnetic fields cannot be ignored and, in fact, lead to unique physics. For example, the quadratic Zeeman shift affects the phase diagram [33]. The ratio of quadratic shift to the spin-dependent interaction strength, δ/U_2, controls the physics of this system. Two different regimes emerge—the Zeeman regime for $\delta>U_2$ and the interaction regime for $\delta<U_2$ [12].

Figure 3 shows an analysis of spin-mixing oscillations $\langle\hat{n}_{m=0}\rangle$ in the presence of a quadratic Zeeman shift δ during the initial state preparation and during the evolution. The other parameters are as in Fig. 1. To highlight the effects of a magnetic field, we show a comparison of the dynamics for $\delta/U_2=0,0.5,1.5,2.5$, and 5 in Fig. 3(a). We see that the oscillations become faster while simultaneously the amplitudes get smaller for increasing δ in the Zeeman regime $\delta>U_2$. The spin-mixing dynamics vanish for a large enough B field. In panel (b) we plot their frequency spectra, comparing the frequencies and the amplitudes. The inset shows two dominant frequencies as a function of the Zeeman strength. A closer look at panel (b) reveals that for a δ in the interaction regime $\delta<U_2$, the dominant frequency initially decreases before starting to increase, due to a competition between the spin-dependent interaction and the Zeeman term. Much of the B-field effects

can be understood from the eigenvalues of H^{final} calculated in the Fock state basis [24] using conservation of atom number and magnetization. For up to three atoms per lattice site, this involves diagonalizing at most a 2×2 matrix. The energy splitting of the eigenvalues of the 2×2 matrices can thus be calculated. In fact, from top to bottom the two curves in the inset of panel (b) are due to contributions from three-atom and two-atom Fock states. In a condensate with large particle numbers, the competition between interaction and Zeeman energy gives rise to a sharp phase boundary at $\delta = U_2$ which can be manifested through magnetic-field-induced resonances [59].

IV. DYNAMICS OF A FERROMAGNETIC SPINOR

A. Evolution without magnetic field

Figure 4 shows the dynamics when our initial state is a ferromagnetic superfluid state of ^{87}Rb with $U_2 < 0$ created in a shallow lattice. For a ferromagnetic state, the collective spin configuration is such that the spin-dependent interaction energy is maximized. This means that the ground state is a superposition of magnetization states in the angular momentum basis $|n,F,M\rangle$ with variance $\Delta m \neq 0$, although it still has magnetization $\langle \hat{m} \rangle = 0$. The parameters are $\langle \hat{n} \rangle = 1.84$, $U_0/(zJ) = 2$, and $U_2 = -0.005U_0$ in the shallow lattice and $U_0 = 0.1\hbar\omega_f$ and $U_2 = -0.005U_0$ in the final deep lattice. The population dynamics $\langle \hat{n}_m \rangle$ is shown in Fig. 4(a). The oscillation amplitude is not as large as in the polar case in the previous section. There are two reasons for this: First, the ground state has comparable populations in all three components and therefore, the population difference between the spin components is smaller to begin with, unlike for ^{23}Na where initially only the $m = 0$ state is occupied. Second, the initial state is much closer to the ground state in the deep lattice. We would like to point out that the smallness of the ferromagnetic interaction is not responsible for the oscillation amplitudes being small. A Fourier analysis in panel (b) of the $m = 0$ population shows that the frequencies present are $3U_2/h, 5U_2/h$, and $7U_2/h$, as in the polar state. Again, energy differences obtained from Eq. (5) give us those frequencies. These frequencies and their spectral weight determine the composition of different Fock components in the initial many-body state and therefore can be used as an experimental probe. We will show in the next subsection that adding magnetic fields can enhance the amplitude of spin-mixing dynamics.

The visibility $|\langle a_{m=0}(t)\rangle|^2/|\langle a_{m=0}(t=0)\rangle|^2$ is shown in Fig. 4(c). It has a simpler pattern than for the polar case in Fig. 2. The coherence of the initial matter wave exhibits collapse and revival modulations with a fast time scale of h/U_0. Its frequency spectrum in panel (d) shows two dominant frequencies, $(U_0 - U_2)/h$ and $2(U_0 - U_2)/h$, although other frequencies with extremely small amplitudes do exist. For ^{87}Rb the dominant frequencies are 199 and 398 in units of U_2/h. As explained for ^{23}Na, these frequencies appear from the overlap of Fock states connected by the annihilation operator $\hat{a}$ [36]. Here, the peak at $(U_0 - U_2)/h$ appears due to the overlap of number states $|0,1,0\rangle$ and $|0,2,0\rangle$. Similarly, the peak at $2(U_0 - U_2)/h$ appears due to number states $|0,2,0\rangle$ and $|0,3,0\rangle$. As with ^{23}Na, finding these frequencies yields a method to experimentally determine U_2/U_0. Nevertheless, since we need to observe many oscillations, ≈200 for ^{87}Rb and ≈80 for ^{41}K, this will be a challenging application of quantum-phase-revival spectroscopy.

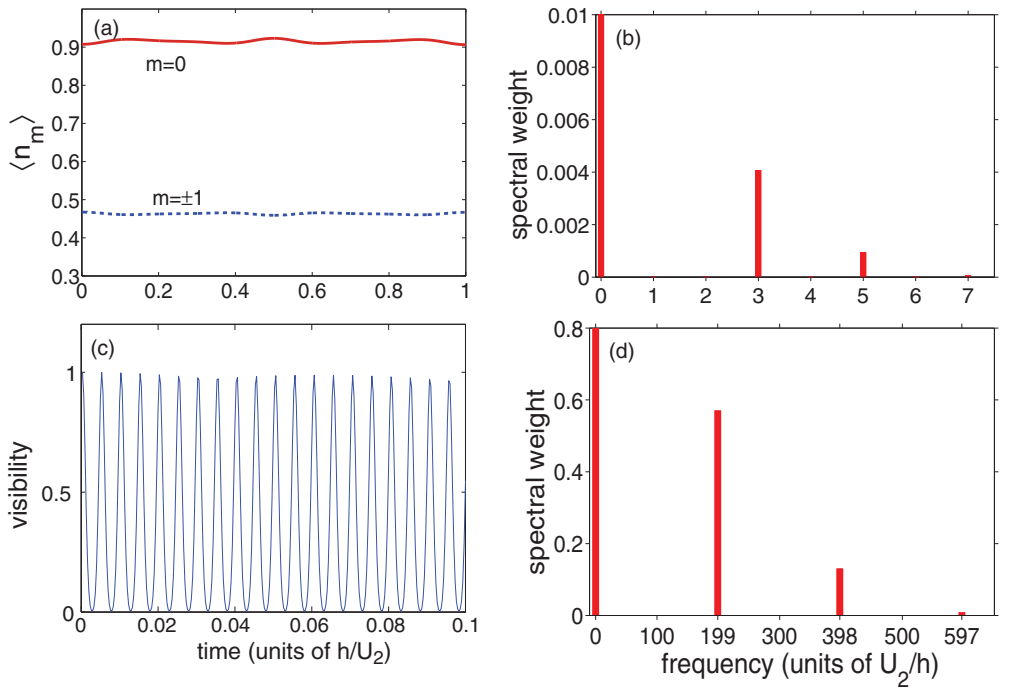

FIG. 4. (Color online) (a) Spin-mixing dynamics $\langle \hat{n}_m \rangle$ for a ferromagnetic $U_2 < 0$ rubidium condensate as a function of hold time. (b) Fourier spectrum showing the relevant frequencies of $3U_2/h$, $5U_2/h$, and $7U_2/h$, and their relative amplitudes. (c) Visibility $|\langle a_{m=0}(t)\rangle|^2/|\langle a_{m=0}(t=0)\rangle|^2$ as a function of hold time. (d) Frequency spectrum of the visibility showing features at $(U_0 - U_2)/h$ and $2(U_0 - U_2)/h$, pointing a way to measure interaction ratios U_2/U_0 from the visibility spectrum.

B. Effects of magnetic field

In this section we study the effects of the quadratic Zeeman interaction on a ferromagnetic spinor. In Fig. 5 we plot spin population $\langle \hat{n}_{m=0} \rangle$ and *in situ* transverse magnetization $|\langle \hat{\mathcal{F}}_x \rangle|^2$ for ^{87}Rb. The parameters are $\langle \hat{n} \rangle = 1.31$, $U_0/(zJ) = 2$, and $U_2 = -0.005U_0$ in the shallow lattice, and $U_0 = 0.1\hbar\omega_f$ and $U_2 = -0.005U_0$ in the final deep lattice. In plots (a) and (b) we show spin-mixing dynamics when the quadratic Zeeman shift is $\delta = U_2$ and $1.5U_2$, respectively. In all the cases, the oscillations are no longer periodic in h/U_2, but the values of δ, U_0, and U_2, combined with the initial state composition, influence the dynamics. We find that the spin-mixing modulation amplitudes become large in the presence of a B field, unlike the antiferromagnetic case in the previous section. The oscillations also get faster, and the fast spin oscillations are modified by an envelope of a slower modulation pattern which is manifested in a beatlike pattern involving the two dominant frequencies, as clearly evident in Fig. 5(b). As we increase δ, the population differences in the $m = 0$ and $m = \pm 1$ states become larger, and therefore large spin-mixing modulations can occur.

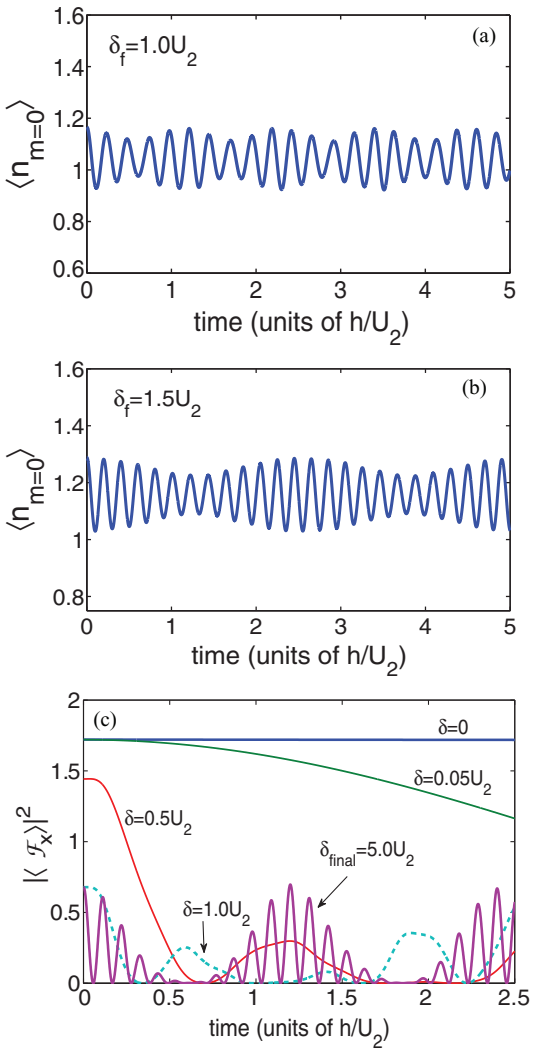

FIG. 5. (Color online) Effect of quadratic Zeeman interactions for ^{87}Rb dynamics. (a, b) Spin-mixing dynamics of the $m = 0$ state for $\delta = U_2$ and $1.5U_2$, respectively. (c) *In situ* transverse magnetization $|\langle \mathcal{F}_x \rangle|^2$ oscillations for various values of δ. Spin-mixing and $|\langle \mathcal{F}_x \rangle|^2$ oscillations depend on a combination of δ, U_2, and the initial state. We see that the spin-mixing amplitudes increase as we increase the field. For transverse magnetization, dynamics is related to how big δ is compared to U_2. When $\delta_f \gg U_2$, where δ_f is the final value during the evolution, it starts to show regular oscillations, as we illustrate in the figure.

Transverse magnetization $|\langle \hat{\mathcal{F}}_x \rangle|^2$ in panel (c) shows that it behaves differently in two regimes. We slowly increase δ and show how it changes the dynamics. For small values of δ, the initial amplitude is large but it decays and oscillates without completely reviving. However, there is a pattern for the modulations when $\delta_f \gg U_2$; here δ_f is the final value of the field during the evolution, rather than its value throughout. In this type of quench when the final evolution is mainly due to a large magnetic field, the periodic oscillations can be explained by the B-field induced equidistant energy spectrum. However, the oscillations for $\delta = 0.5U_2$ and $\delta = 1.0U_2$ slowly deviate from the two opposing limits of $\delta = 0$ and $\delta \gg U_2$, and have complete collapse but partial revivals. Faraday rotation spectroscopy can be used to detect transverse magnetizations [2]. This could give us a direct probe of the magnetic properties in our quench setup, in addition to the coherence properties which we can obtain through population and visibility revivals.

V. SIGNATURE OF EFFECTIVE THREE-BODY INTERACTIONS

A. Three-body interactions

In our dynamical scheme, the evolution of the many-body state takes place in a deep optical lattice with no tunneling to the neighbors. In such a setting, even within the single-band Bose-Hubbard model, there are effective three- and higher-body interactions due to collision-induced virtual excitations to higher bands or vibrational levels. For the spinless bosonic case, such effective multibody interactions have been predicted in theory [37]. A recent experiment [36] monitored matter-wave collapse and revival dynamics for tens of oscillations and observed the signature of higher-body effects in the visibility time trace. A more accurate treatment of a multicomponent system in a deep lattice should therefore also incorporate higher-band induced multibody interaction terms. Three-body interactions can be important for Efimov physics [60] and for many-particle systems, giving rise to novel and exotic phenomena [61–64].

In a deep lattice, the minimum of the potential at a single site can be approximated as a harmonic potential. For spin-1 bosons in a single isotropic harmonic trap, the derivation of the effective three-body interactions is given in the Appendix. The effect can be concisely represented by adding

$$H_{3\mathrm{B,eff}} = \frac{V_0}{6}\hat{n}(\hat{n}-1)(\hat{n}-2) + \frac{V_2}{6}(\vec{\mathcal{F}}^2 - 2\hat{n})(\hat{n}-2) \quad (6)$$

to H^{final} in Eq. (4). Here, as previously, $\hat{n} = \hat{n}_{-1} + \hat{n}_0 + \hat{n}_1$ is the on-site atom number and $\vec{\mathcal{F}} = \sum_{m,m'} a_m^\dagger \vec{F}_{mm'} a_{m'}$ is the on-site total angular momentum. The Hamiltonian term with strength V_0 is similar to the spin-0 effective three-body interaction of Refs. [37] and [36] and depends only

on total particle number. The new Hamiltonian term with strength V_2 depends intricately on the atomic spin. For a harmonic potential with frequency ω_f, V_0 is attractive and equal to $V_0 = -1.34U_0^2/(\hbar\omega_f)$ [37]. The strength V_2 satisfies $V_2 = 2(U_2/U_0)V_0$. There is no magnetic field dependence in the effective three-body terms. Finally, we note that the perturbative effective three-body Hamiltonian is only valid when the three-body interaction strengths (V_0, V_2) are much smaller than the corresponding two-body strengths (U_0, U_2).

The on-site effective Hamiltonian $H_{3\mathrm{B,eff}}$ is diagonal in the angular momentum basis states $|n, F, M\rangle$ with diagonal matrix elements:

$$E_{3\mathrm{B,eff}} = \frac{V_0}{6}n(n-1)(n-2) + \frac{V_2}{6}[F(F+1) - 2n](n-2), \tag{7}$$

with the same restrictions as in Eq. (5) on allowed values of F. Equation (7) is one of the key results in this paper. This spectrum extends and generalizes the spectrum of the spin-mixing spinor Hamiltonian as presented in Ref. [14] to the effective three-body case. As discussed next, this helps us quantify and understand the effects of three-body interactions on our dynamics scenario.

B. Effects on dynamics

For spinless bosons in an optical lattice, a time-of-flight measurement of the visibility dynamics determined the strength of the effective multibody interactions [36,52]. Here for spin-1 bosons in an optical lattice, we show that the effective three-body interaction effects can be observed directly in the on-site population density—in the spin oscillation dynamics. This opens up the possibility that *in situ* measurements such as using quantum microscopes [54,65] and other techniques [66] in lattices could be used to detect effective multibody interactions. Because of the more complex nature of visibility patterns, we only analyze spin-mixing population dynamics.

In Fig. 6 we show the effects of the effective three-body interactions in the spin-mixing dynamics of an initial polar superfluid state of ^{23}Na at $U_0/(zJ) = 2$, $U_2 = 0.04U_0$, and $\delta = 0$. The occupation is $\langle\hat{n}\rangle = 2.35$, which highlights the three-body effects, and $\langle\hat{m}\rangle = 0$. The interaction strengths for the deep lattice are $U_0 = 0.1\hbar\omega_f$ and $U_2 = 0.04U_0$, so that $V_0 = -0.134U_0$ and $V_2 = -0.268U_2$. In an earlier section we have seen that spin-mixing dynamics is controlled by U_2. Here, we find that this spin-mixing scaling is also influenced by the three-body interaction V_2. Figure 6(a) shows a comparison of the dynamics with and without the three-body term. We see that the time traces start to differ after the first oscillation, and the periodicity in h/U_2 is destroyed. A frequency analysis of the oscillations in panel (b) elucidates the exact nature of the modulations. Without a three-body term, strong features appear at $3U_2/h$,$5U_2/h$, and $7U_2/h$. With a three-body term, additional frequencies appear at $2.46U_2/h$,$4.55U_2/h$, and $5.75U_2/h$, which follow from the energy differences of the three-body spectrum in Eq. (7). Identification of any of the frequencies gives us the V_2 coupling strength. For example, the peak at $4.55U_2/h$ arises as the initial state contains contributions of angular momentum states $|3,1,0\rangle$ and $|3,3,0\rangle$ containing three atoms. These two states have an energy

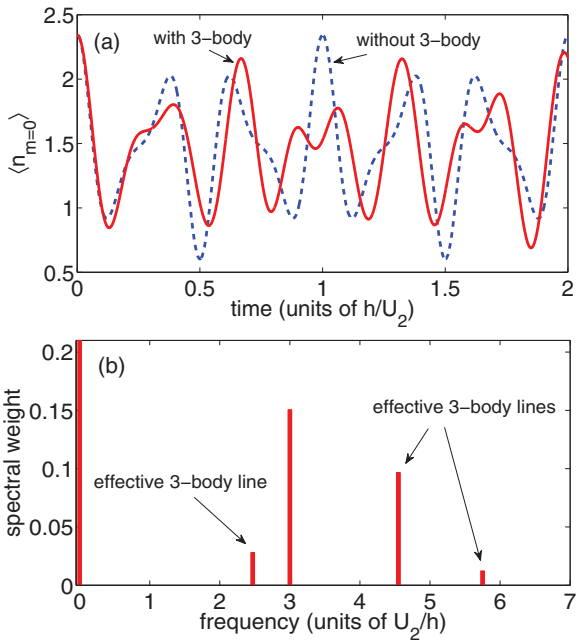

FIG. 6. (Color online) Effects of effective three-body interactions on the spin-mixing dynamics for a polar (^{23}Na) initial state. (a) The population $\langle\hat{n}_{m=0}\rangle$ as a function of hold time for occupation $\langle\hat{n}\rangle = 2.35$ and $\delta = 0$ with (solid line) and without (dashed line) the effective three-body interaction. (b) Frequency analysis of the time trace with effective three-body interactions reveals the presence of additional frequencies, which could be used to determine the three-body interaction strength.

difference of $5U_2 + 5V_2/3$, whose signature is the $4.55U_2/h$ frequency.

In experiments an unknown effective three-body strength V_2 can be deduced by assigning several frequencies in the time trace. The presence of all the other frequencies can be used to reduce error in the measurement and verify the spectrum Eq. (7). The spectral weights and the values of the frequencies also give us clues about the initial superfluid state. Control of initial squeezing [36,52], by varying $U_0/(zJ)$ in the shallow lattice, can be used in such a way that some of the frequencies are more dominant, so as to make detection easier.

In Fig. 7 we show the spin dynamics $\langle\hat{n}_{m=0}\rangle$ for a ferromagnetic (^{87}Rb) initial state at $U_0/(zJ) = 2$, $\delta = 0$, $\langle\hat{m}\rangle = 0$, and $\langle\hat{n}\rangle = 2.35$ in the shallow lattice. In the deep lattice we use $U_0 = 0.1\hbar\omega_f$ and $U_2 = -0.005U_0$. The spin-mixing amplitude is not that prominent for ^{87}Rb. Nevertheless, the influence of the three-body interaction is discernible in our simulation. The frequency spectrum of the time trace shown in (b) makes it clear that new frequencies emerge at $4.55U_2/h$ and $5.75U_2/h$, proving the existence of three-body interactions and yielding a method to measure its strength. The appearance of additional frequencies is similar to the ^{23}Na case, except that we do not observe a feature at $2.46U_2/h$, which is due to a coherence between four-atom angular momentum states $|4,0,0\rangle$ and $|4,2,0\rangle$. For the ferromagnetic initial superfluid, the angular momentum state $|4,0,0\rangle$ is absent. It is conceivable that initial squeezing control of a ground state [36,52] or other specific initial state preparations [14,15] can be used to see larger amplitude spin-mixing oscillations to make

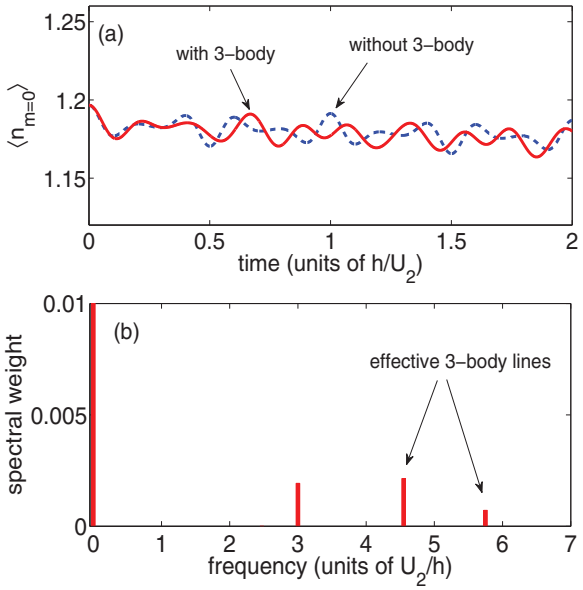

FIG. 7. (Color online) Effects of effective three-body interactions on the spin-mixing dynamics for a ferromagnetic (^{87}Rb) initial state. (a) The population $\langle \hat{n}_{m=0} \rangle$ as a function of hold time with (solid line) and without (dashed line) the three-body interaction. For ^{87}Rb the oscillation amplitude is small. (b) Frequency analysis reveals the presence of several frequencies, which are a signature of induced three-body interactions; compared to ^{23}Na in Fig. 6, one frequency is missing for ^{87}Rb due to its ferromagnetic nature.

the experimental detection of three-body effects easier for ferromagnetic coupling.

VI. CONCLUSION

In this paper we performed a theoretical study of the dynamics of spin-1 bosons in an optical lattice in a quench scenario where we start from a ground state in a shallow lattice and suddenly raise the lattice depth. We have shown that the ensuing spin-mixing and visibility oscillations can be used as a probe of the initial superfluid ground state. The spectral analysis of time evolution reveals the Fock state composition of the initial state and thereby its superfluid and magnetic properties. Analysis of visibility oscillations, i.e., quantum-phase-revival spectroscopy, further yields a method to determine the spin-dependent and spin-independent interaction ratio U_2/U_0, which is an important quantity for spinor gases. We treat both antiferromagnetic (e.g., ^{23}Na atoms) and ferromagnetic (e.g., ^{87}Rb) condensates. For ferromagnetic interactions the spin-mixing oscillation amplitudes are small. When external magnetic field cannot be ignored, the inclusion of a quadratic Zeeman field is necessary, and we have quantified such dynamics. We have shown that the presence of a magnetic field increases the spin-mixing amplitude for a ferromagnetic condensate.

The Hamiltonian that more accurately describes the physics of the final deep lattice is comprised of two-body as well as effective multibody interactions, which arise due to virtual excitations to higher bands. We derive the induced three-body interaction parameters for spin-1 atoms in a deep harmonic well and show its effect on the spin-mixing dynamics. We demonstrate that a frequency analysis of the oscillations can detect the signature and strength of the spin-dependent three-body interactions. We stress our finding that the three-body interactions for spinor atoms can be observed directly in the *in situ* number densities, in addition to the time-of-flight visibility, as observed for spinless bosons [36].

Our analysis here is based on various approximations. Our initial state is a mean-field product state which neglects quantum and thermal fluctuations. Our calculations with spin-0 bosons [67] suggest that quantum fluctuations change the composition of the initial state slightly but do not affect the dynamics significantly, as the sites are completely decoupled and on-site density fluctuations are frozen. Thermal fluctuations, on the other hand, cause the visibility dynamics to slowly decay. This would make it hard for the experimentalists to follow the dynamics for a long time. None of our basic conclusions in this paper are negated by these effects. For a more complete understanding of our model, future work should include these corrections. In experiments three-body loss can be an important factor. However, the atom density is small enough that the dynamics for spinless bosons have been followed for many oscillations [36] without significant loss. Three-body recombination should be included in our analysis if the dynamics are to be followed over a longer period than currently observed.

In addition to the effective three-body interactions, there can be four-body and higher-order terms. Spin-independent four-body terms are not negligible compared to the spin-dependent three-body interactions, and can influence the visibility dynamics, as seen in spin-0 collapse and revival experiments [36]. However, in this paper we demonstrate that the signature of three-body spin-dependent interaction shows up in spin-mixing density dynamics, and this signal is not affected by any spin-independent interactions. Long-range dipolar interactions can be an important energy scale for atoms such as Cr and Dy. For Na and Rb discussed in our paper, the dipolar interactions are small and our estimate suggests that they are an order of magnitude smaller than spin-dependent three-body interaction.

Although there have been many theoretical studies for spin-1 bosons in an optical lattice, a many-body correlated ground state has not yet been achieved experimentally. There are many unexplored questions in that regard. Here, we have combined the study of dynamics with optical lattice spinors to show how nonequilibrium dynamics can be used as a probe for revealing ground-state properties and spinor interactions. There are other dynamic scenarios that can give different perspectives on spinor lattice physics, such as a quench from Mott insulator to superfluid and evolution in a tunnel coupled lattice, to name a couple. The interplay of superfluidity, magnetism, and strong correlations makes this a rich system where the study of quantum dynamics may lead to a better understanding of collective phenomena.

ACKNOWLEDGMENTS

K.W.M. would like to thank Richard Scalettar and Hulikal Krishnamurthy for helpful discussions during the early stages of this work. We acknowledge support from the US Army Research Office under Contract No. 60661PH and the National

Science Foundation Physics Frontier Center located at the Joint Quantum Institute.

APPENDIX: EFFECTIVE THREE-BODY SPINOR INTERACTIONS

In this Appendix we derive the effective three-body spinor interaction due to virtual excitations to excited trap levels of the isolated sites of the deep optical lattice. The derivation closely follows Refs. [37] and [52]. Atoms are held in the ground state of a site, which we approximate by an isotropic 3D harmonic-oscillator potential with frequency ω_f. Then the Hamiltonian for spin-1 bosons is $H = H_0 + \mathcal{V}_0 + \mathcal{V}_2$ with

$$H_0 = (\epsilon_\alpha + m^2\delta)a^\dagger_{m\alpha}a_{m\alpha}, \tag{A1}$$

$$\mathcal{V}_0 = \tfrac{1}{2}c_0 g_{\alpha\beta,\gamma\delta}a^\dagger_{k\alpha}a^\dagger_{l\beta}a_{k\alpha}a_{l\beta}, \tag{A2}$$

$$\mathcal{V}_2 = \tfrac{1}{2}c_2 g_{\alpha\beta,\gamma\delta}a^\dagger_{k\alpha}a^\dagger_{l\beta}(\vec{F}_{km}\cdot\vec{F}_{ln})a_{m\gamma}a_{n\delta}\,, \tag{A3}$$

where operators $a_{m\alpha}$ annihilate an atom in spin projection $m = -1,0,1$ and 3D harmonic oscillator state α. We use the convention that Roman and Greek subscripts represent spin projections and harmonic oscillator states, respectively. Repeated indices are summed over. The single-particle energies ϵ_α and $m^2\delta$ are the harmonic oscillator and quadratic Zeeman energies, respectively. For the ground state $\alpha = 0$. We choose $\epsilon_0 = 0$ and will require that $\epsilon_\alpha - \epsilon_0 \gg \delta$ for $\alpha \neq 0$. The spin-independent and spin-dependent atom-atom interactions V_0 and V_2 have "bare-coupling" strengths c_0 and c_2, respectively. The vector $\vec{F} = (F_x, F_y, F_z)$ are spin-1 matrices. Each symmetric real coefficient $g_{\alpha\beta,\gamma\delta}$ is a 3D integral over the product of the four oscillator wave functions α, β, γ, and δ. In this Appendix the two atom-atom interactions are explicitly normal-ordered in order to facilitate the derivation.

We can now derive the effective Hamiltonian with atoms in the lowest oscillator state using degenerate perturbation theory with zeroth-order Hamiltonian H_0 and perturbation $\mathcal{V}_0 + \mathcal{V}_2$. First, we define for every spatial mode α the spin wave function $|\{n_{-1},n_0,n_1\}_\alpha\rangle$ with $n_m = 0,1,2,\ldots$ atoms in spin state m. The ground states P are formed by the orthonormal basis functions $|g\rangle = |\{n_{-1},n_0,n_1\}_0,0_{\alpha\neq0}\rangle$ for any value of n_m and where $0_{\alpha\neq0}$ indicates that there are no atoms in excited spatial modes. Their energy is $E_g = (n_{-1}+n_1)\delta$. Excited states $|e\rangle$ with energy E_e are states where at least one atom occupies a $\alpha \neq 0$ spatial mode.

We reproduce the Hamiltonian in Eq. (4) in first-order perturbation theory once we make the assignment $U_0 = c_0 g_{00,00}$ and $U_2 = c_2 g_{00,00}$. To second order in degenerate perturbation theory the matrix element for ground motional states $|g'\rangle$ and $|g\rangle$ is

$$\langle g'|\delta H^{(2)}|g\rangle = \frac{1}{2}\sum_{e\neq P}\langle g'|\mathcal{V}_0+\mathcal{V}_2|e\rangle \times\left\{\frac{1}{E_g-E_e}+\frac{1}{E_{g'}-E_e}\right\}\langle e|\mathcal{V}_0+\mathcal{V}_2|g\rangle\,. \tag{A4}$$

The sum over excited states can be evaluated by realizing that only states $|e\rangle \propto a^\dagger_{k\alpha}a^\dagger_{l\beta}a_{m0}a_{n0}|g\rangle$ with $\alpha\beta \neq 00$ and $k+l = m+n$ contribute, as both $\mathcal{V}_0$ and $\mathcal{V}_2$ conserve atom number and magnetization and can only change the state of two atoms at the same time, i.e., states $|e\rangle$ are those with at most two atoms in the higher trap levels. By inspection, we then realize that the energy differences $E_e - E_g \approx \epsilon_\alpha + \epsilon_\beta$ are independent of the total number of atoms in the ground states and to good approximation are also independent of the quadratic Zeeman energy, as $\delta \ll \epsilon_\alpha$ for $\alpha \neq 0$. Similar expressions hold for $E_e - E_{g'}$.

Inserting the (normalized) expression for $|e\rangle$ and performing the sums over $|e\rangle$ as well as those appearing in the potentials $\mathcal{V}_0$ and $\mathcal{V}_2$, we first find

$$\langle g'|\delta H^{(2)}|g\rangle = -\sum_{\alpha\beta\neq00,\mu\nu} g_{00,\mu\nu}\frac{1}{\epsilon_\alpha+\epsilon_\beta}g_{\alpha\beta,00} \times\left\{\frac{1}{4}c_0^2\langle g'|a^\dagger_{m0}a^\dagger_{n0}a_{m\mu}a_{n\nu}a^\dagger_{k\alpha}a^\dagger_{l\beta}a_{k0}a_{l0}|g\rangle + \frac{1}{2}c_0c_2\langle g'|a^\dagger_{p0}a^\dagger_{o0}(\vec{F}_{pm}\cdot\vec{F}_{on})a_{m\mu}a_{n\nu}a^\dagger_{k\alpha}a^\dagger_{l\beta}a_{k0}a_{l0}|g\rangle\right\}, \tag{A5}$$

where the remaining sums over trap levels have been made explicit, repeated roman indices are still summed over, and we have omitted the contribution proportional to $V_2 \times V_2$, as the spin-dependent interaction strength is an order of magnitude smaller than the spin-independent one.

By normal ordering the creation and annihilation operators in Eq. (A5) and using the fact that ground states P contain no atoms in excited trap levels, we find

$$\langle g'|\delta H^{(2)}|g\rangle = \langle g'|\delta H_{2B} + H_{3B}|g\rangle\,, \tag{A6}$$

where

$$\delta H_{2B} = Z_2\left\{-\frac{1}{2}c_0^2a^\dagger_{k0}a^\dagger_{l0}a_{k0}a_{l0} - c_0c_2a^\dagger_{m0}a^\dagger_{n0}(\vec{F}_{mk}\cdot\vec{F}_{nl})a_{k0}a_{l0}\right\} \tag{A7}$$

is a correction to the pairwise two-body interaction and

$$H_{3B} = Z_3\left\{-c_0^2a^\dagger_{k0}a^\dagger_{l0}a^\dagger_{m0}a_{k0}a_{l0}a_{m0} -2c_0c_2a^\dagger_{o0}a^\dagger_{m0}a^\dagger_{n0}(\vec{F}_{mk}\cdot\vec{F}_{nl})a_{k0}a_{l0}a_{o0}\right\} \tag{A8}$$

is an effective three-body interaction. Here

$$Z_2 = \sum_{\mu\nu\neq00} g_{00,\mu\nu}\frac{1}{\epsilon_\mu+\epsilon_\nu}g_{\mu\nu,00} \tag{A9}$$

and

$$Z_3 = \sum_{\mu\neq0} g_{00,\mu0}\frac{1}{\epsilon_\mu}g_{\mu0,00}\,. \tag{A10}$$

The sums in Z_2 diverge and must be regularized and renormalized [52,68]. That is, we require that the bare coupling constant c_0 is defined such that, by combining the first- and second-order contributions, $c_0 g_{00,00} - c_0^2 Z_2$ is finite and equal to U_0. Similarly, we require that $c_2 g_{00,00} - 2c_0c_2Z_2$ is finite and equal to U_2.

The sums in coefficient Z_3 of the effective three-body Hamiltonian do converge. Hence we redefine the effective three-body interaction as

$$H_{3B} = \frac{1}{6}V_0\, a^\dagger_{k0}a^\dagger_{l0}a^\dagger_{m0}a_{k0}a_{l0}a_{m0} + \frac{1}{6}V_2\, a^\dagger_{o0}a^\dagger_{m0}a^\dagger_{n0}(\vec{F}_{mk}\cdot\vec{F}_{nl})a_{k0}a_{l0}a_{o0}\,, \qquad \text{(A11)}$$

where, consistent within our second-order perturbative calculation,

$$V_0 = -6U_0^2\,\frac{1}{g^2_{00,00}}Z_3 \quad\text{and}\quad V_2 = -12U_0U_2\,Z_3 = 2\frac{U_2}{U_0}V_0$$

are the spin-independent and spin-dependent three-body interaction strengths, respectively. For a spherically symmetric harmonic oscillator, $V_0 = -1.34\ldots U_0^2/(\hbar\omega_f)$ [37]. Since $U_2 > 0$ for Na atoms, $V_2 < 0$, while for ^{87}Rb, $U_2 < 0$ and thus $V_2 > 0$.

The two- and three-body interactions can be rewritten in terms of the angular momentum operators $\vec{\mathcal{F}} = (\hat{\mathcal{F}}_x,\hat{\mathcal{F}}_y,\hat{\mathcal{F}}_z)$ defined in Eq. (1) following Ref. [14]. By combining the quadratic Zeeman interaction as well as the two-body and effective three-body interactions, we find our final result:

$$H_{\rm eff} = \delta\sum_m m^2 a^\dagger_m a_m + \frac{1}{2}U_0\hat{n}(\hat{n}-1) + \frac{1}{2}U_2(\vec{\mathcal{F}}^2 - 2\hat{n}) + \frac{1}{6}V_0\hat{n}(\hat{n}-1)(\hat{n}-2) + \frac{1}{6}V_2(\vec{\mathcal{F}}^2-2\hat{n})(\hat{n}-2)\,,$$

where we suppressed the ground-state oscillator index, and $\vec{\mathcal{F}}^2$ and the number operator $\hat{n}$ commute.

[1] D. M. Stamper-Kurn, M. R. Andrews, A. P. Chikkatur, S. Inouye, H.-J. Miesner, J. Stenger, and W. Ketterle, Phys. Rev. Lett. **80**, 2027 (1998).

[2] Y. Liu, E. Gomez, S. E. Maxwell, L. D. Turner, E. Tiesinga, and P. D. Lett, Phys. Rev. Lett. **102**, 225301 (2009); Y. Liu, S. Jung, S. E. Maxwell, L. D. Turner, E. Tiesinga, and P. D. Lett, *ibid.* **102**, 125301 (2009).

[3] M. Vengalattore, S. R. Leslie, J. Guzman, and D. M. Stamper-Kurn, Phys. Rev. Lett. **100**, 170403 (2008).

[4] D. Jacob, L. Shao, V. Corre, T. Zibold, L. De Sarlo, E. Mimoun, J. Dalibard, and F. Gerbier, Phys. Rev. A **86**, 061601(R) (2012).

[5] A. Vinit, E. M. Bookjans, C. A. R. Sa de Melo, and C. Raman, Phys. Rev. Lett. **110**, 165301 (2013).

[6] H. Schmaljohann, M. Erhard, J. Kronjäger, M. Kottke, S. van Staa, L. Cacciapuoti, J. J. Arlt, K. Bongs, and K. Sengstock, Phys. Rev. Lett. **92**, 040402 (2004).

[7] M.-S. Chang, C. D. Hamley, M. D. Barrett, J. A. Sauer, K. M. Fortier, W. Zhang, L. You, and M. S. Chapman, Phys. Rev. Lett. **92**, 140403 (2004).

[8] T. Kuwamoto, K. Araki, T. Eno, and T. Hirano, Phys. Rev. A **69**, 063604 (2004).

[9] L. Santos and T. Pfau, Phys. Rev. Lett. **96**, 190404 (2006).

[10] B. Pasquiou, E. Maréchal, G. Bismut, P. Pedri, L. Vernac, O. Gorceix, and B. Laburthe-Tolra, Phys. Rev. Lett. **106**, 255303 (2011).

[11] T. L. Ho, Phys. Rev. Lett. **81**, 742 (1998); T. Ohmi and K. Machida, J. Phys. Soc. Jpn. **67**, 1822 (1998).

[12] D. M. Stamper-Kurn and M. Ueda, arXiv:1205.1888v1.

[13] Y. Kawaguchi and M. Ueda, Phys. Reports **520**, 253 (2012).

[14] C. K. Law, H. Pu, and N. P. Bigelow, Phys. Rev. Lett. **81**, 5257 (1998).

[15] M. Chang, Q. Qin, W. Zhang, L. You, and M. S. Chapman, Nat. Phys. **1**, 111 (2005).

[16] W. Zhang, D. L. Zhou, M.-S. Chang, M. S. Chapman, and L. You, Phys. Rev. Lett. **95**, 180403 (2005).

[17] D. Jaksch, C. Bruder, J. I. Cirac, C. W. Gardiner, and P. Zoller, Phys. Rev. Lett. **81**, 3108 (1998).

[18] M. Greiner, O. Mandel, T. Esslinger, T. W. Hänsch, and I. Bloch, Nature (London) **415**, 39 (2002).

[19] I. Bloch, J. Dalibard, and W. Zwerger, Rev. Mod. Phys. **80**, 885 (2008).

[20] M. Lewenstein, A. Sanpera, V. Ahufinger, B. Damski, A. Sen, and U. Sen, Adv. Phys. **56**, 243 (2007).

[21] J. S. Krauser, J. Heinze, N. Fläshner, S. Götze, O. Jürgensen, D.-S. Lühmann, C. Becker, and K. Sengstock, Nat. Phys. **8**, 813 (2012).

[22] K. Jimenez-Garcia, R. L. Compton, Y.-J. Lin, W. D. Phillips, J. V. Porto, and I. B. Spielman, Phys. Rev. Lett. **105**, 110401 (2010).

[23] K. W. Mahmud, E. N. Duchon, Y. Kato, N. Kawashima, R. T. Scalettar, and N. Trivedi, Phys. Rev. B **84**, 054302 (2011).

[24] A. Widera, F. Gerbier, S. Fölling, T. Gericke, O. Mandel, and I. Bloch, Phys. Rev. Lett. **95**, 190405 (2005); New J. Phys. **8**, 152 (2006).

[25] S. Trotzky, P. Cheinet, S. Fölling, M. Feld, U. Schnorrberger, A. M. Rey, A. Polkovnikov, E. A. Demler, M. D. Lukin, and I. Bloch, Science **319**, 295 (2007).

[26] C. Becker, P. Soltan-Panahi, J. Kronjäger, S. Dörscher, K. Bongs, and K. Sengstock, New. J. Phys. **12**, 065025 (2010).

[27] K. W. Mahmud, G. G. Batrouni, and R. T. Scalettar, Phys. Rev. A **81**, 033609 (2010).

[28] E. Demler and F. Zhou, Phys. Rev. Lett. **88**, 163001 (2002).

[29] M. Snoek and F. Zhou, Phys. Rev. B **69**, 094410 (2004).

[30] A. Imambekov, M. Lukin, and E. Demler, Phys. Rev. A **68**, 063602 (2003); Phys. Rev. Lett. **93**, 120405 (2004).

[31] G. G. Batrouni, V. G. Rousseau, and R. T. Scalettar, Phys. Rev. Lett. **102**, 140402 (2009).

[32] R. V. Pai, K. Sheshadri, and R. Pandit, Phys. Rev. B **77**, 014503 (2008).

[33] K. Rodríguez, A. Argüelles, A. K. Kolezhuk, L. Santos, and T. Vekua, Phys. Rev. Lett. **106**, 105302 (2011).

[34] A. Polkovnikov, K. Sengupta, A. Silva, and M. Vengalattore, Rev. Mod. Phys. **83**, 863 (2011).

[35] M. Greiner, O. Mandel, T. W. Hänsch, and I. Bloch, Nature (London) **415**, 51 (2002).

[36] S. Will, T. Best, U. Schneider, L. Hackermüller, D.-S. Lühmann, and I. Bloch, Nature (London) **465**, 197 (2010).
[37] P. R. Johnson, E. Tiesinga, J. V. Porto, and C. J. Williams, New J. Phys. **11**, 093022 (2009).
[38] L. E. Sadler, J. M. Higbie, S. R. Leslie, M. Vengalattore, and D. M. Stamper-Kurn, Nature (London) **443**, 312 (2006).
[39] M. Vengalattore, J. M. Higbie, S. R. Leslie, J. Guzman, L. E. Sadler, and D. M. Stamper-Kurn, Phys. Rev. Lett. **98**, 200801 (2007).
[40] E. M. Bookjans, C. D. Hamley, and M. S. Chapman, Phys. Rev. Lett. **107**, 210406 (2011).
[41] J. Sebby-Strabley, B. L. Brown, M. Anderlini, P. J. Lee, W. D. Phillips, J. V. Porto, and P. R. Johnson, Phys. Rev. Lett. **98**, 200405 (2007).
[42] S. Knoop, T. Schuster, R. Scelle, A. Trautmann, J. Appmeier, M. K. Oberthaler, E. Tiesinga, and E. Tiemann, Phys. Rev. A **83**, 042704 (2011).
[43] E. G. M. van Kempen, S. J. J. M. F. Kokkelmans, D. J. Heinzen, and B. J. Verhaar, Phys. Rev. Lett. **88**, 093201 (2002).
[44] M. Lysebo and L. Veseth, Phys. Rev. A **81**, 032702 (2010).
[45] S. Falke, H. Knöckel, J. Friebe, M. Riedmann, E. Tiemann, and C. Lisdat, Phys. Rev. A **78**, 012503 (2008).
[46] M. Rizzi, D. Rossini, G. DeChiara, S. Montangero, and R. Fazio, Phys. Rev. Lett. **95**, 240404 (2005); S. Bergkvist, I. P. McCulloch, and A. Rosengren, Phys. Rev. A **74**, 053419 (2006).
[47] K. V. Krutitsky and R. Graham, Phys. Rev. A **70**, 063610 (2004); K. V. Krutitsky, M. Timmer, and R. Graham, *ibid.* **71**, 033623 (2005).
[48] T. Kimura, S. Tsuchiya, and S. Kurihara, Phys. Rev. Lett. **94**, 110403 (2005); S. Tsuchiya, S. Kurihara, and T. Kimura, Phys. Rev. A. **70**, 043628 (2004).
[49] K. Sheshadri, H. R. Krishnamurthy, R. Pandit, and T. V. Ramakrishnan, Europhys. Lett. **22**, 257 (1993).
[50] D. van Oosten, P. van der Straten, and H. T. C. Stoof, Phys. Rev. A **63**, 053601 (2001).
[51] D. M. Brink and G. R. Satchler, *Angular Momentum*, 3rd ed. (Clarendon Press, Oxford, 1993).
[52] E. Tiesinga and P. R. Johnson, Phys. Rev. A **83**, 063609 (2011).
[53] J. Schachenmayer, A. J. Daley, and P. Zoller, Phys. Rev. A **83**, 043614 (2011).
[54] W. S. Bakr, J. I. Gillen, A. Peng, S. Foelling, and M. Greiner, Nature (London) **462**, 74 (2009).
[55] S. Will, T. Best, S. Braun, U. Schneider, and I. Bloch, Phys. Rev. Lett. **106**, 115305 (2011).
[56] A. T. Black, E. Gomez, L. D. Turner, S. Jung, and P. D. Lett, Phys. Rev. Lett. **99**, 070403 (2007).
[57] W. Zhang, D. L. Zhou, M.-S. Chang, M. S. Chapman, and L. You, Phys. Rev. A **72**, 013602 (2005).
[58] Q. Zhai, L. Chang, R. Lu, and L. You, Phys. Rev. A **79**, 043608 (2009).
[59] J. Kronjager, C. Becker, P. Navez, K. Bongs, and K. Sengstock, Phys. Rev. Lett. **97**, 110404 (2006).
[60] E. Braaten and H.-W. Hammer, Ann. Phys. **322**, 120 (2007).
[61] B. Paredes, T. Keilmann, and J. I. Cirac, Phys. Rev. A **75**, 053611 (2007).
[62] B. Capogrosso-Sansone, S. Wessel, H. P. Büchler, P. Zoller, and G. Pupillo, Phys. Rev. B **79**, 020503 (2009).
[63] L. Mazza, M. Rizzi, M. Lewenstein, and J. I. Cirac, Phys. Rev. A **82**, 043629 (2010).
[64] T. Sowinski, Phys. Rev. A **85**, 065601 (2012); T. Sowinski *et al.*, arXiv:1304.4835.
[65] J. Simon, W. S. Bakr, R. Ma, M. E. Tai, P. M. Preiss, and M. Greiner, Nature (London) **472**, 307 (2011).
[66] N. Gemelke, X. Zhang, C. Hung, and C. Chin, Nature (London) **460**, 995 (2009).
[67] K. W. Mahmud and E. Tiesinga (unpublished).
[68] A. Fetter and J. D. Walecka, *Quantum Theory of Many-Particle Systems* (McGraw-Hill, New York, 1971).